

# QCD perturbation theory at finite temperature/density and its application

M.H. Thoma<sup>a\*</sup>

<sup>a</sup>Institut für Theoretische Physik, Universität Giessen,  
35392 Giessen, Germany

In order to describe properties of an equilibrated quark-gluon plasma, QCD at finite temperature (and density) has to be considered. Besides lattice calculations, which can be applied only to static quantities at zero density, perturbative QCD has been used. At finite temperature, however, serious problems such as infrared divergent and gauge dependent results have been encountered. These difficulties can be (partially) avoided if one starts from effective Green functions constructed by resumming a certain class of diagrams (hard thermal loops). Within the last few years this improved perturbation theory (Braaten-Pisarski method) turned out to be a powerful tool for computing interesting quantities of the quark-gluon plasma phase.

In the present talk a basic introduction to the Braaten-Pisarski method is provided and its applications and limits are reviewed. In particular, damping rates, the energy loss of energetic partons, thermalization times, the viscosity of the quark-gluon plasma, and the production of photons and dileptons are discussed.

## 1. FINITE TEMPERATURE FIELD THEORY

In order to detect a quark-gluon plasma (QGP) possibly produced in ultrarelativistic heavy ion collisions, we are dependent on a thorough understanding of the properties of a QGP and a prediction of signatures for the QGP formation. For this purpose we are forced to use QCD at finite temperature and chemical potential, since the QGP is a relativistic quantum systems of partons at finite temperature and baryon density. There are basically two approaches to this problem.

The first one is lattice QCD [1], which is able to describe a strong interacting system at all temperatures from below to above the phase transition from hadronic matter to a QGP. However, so far lattice QCD cannot be used to compute dynamical quantities such as particle productions from the QGP. Also systems at finite density or out of equilibrium cannot be treated in this way.

The second approach is perturbative QCD at finite temperature. It is based on the fact that due to asymptotic freedom the effective temperature dependent strong coupling constant  $\alpha_s(T) = g^2/4\pi$  becomes small at high temperature. For example, at  $T = 250$  MeV the coupling constant is expected to assume values of the order  $\alpha_s = 0.3 - 0.5$ . To

---

\*Heisenberg fellow

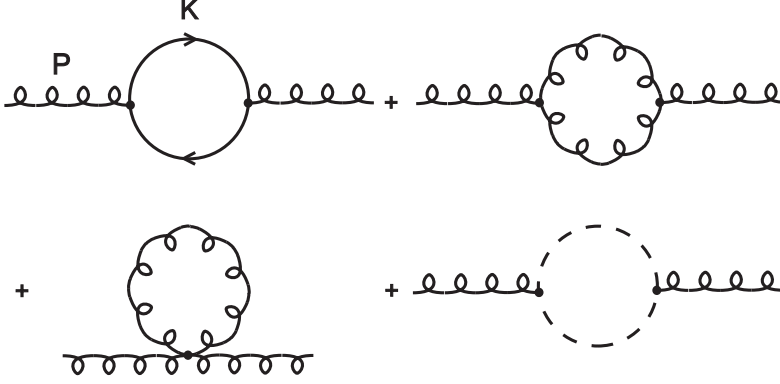


Figure 1. HTL gluon self energy containing quark, gluon, and ghost loops.

which extent perturbation theory works for realistic situations, which can be realized in heavy ion collisions, will be discussed at the end of this talk.

Applying perturbative QCD at high temperatures static as well as dynamical quantities of a QGP can be considered. Also it is straightforward to extend this method to finite quark chemical potential. Furthermore the application of perturbative QCD to non-equilibrium situations, expected to take place in the first stage of a relativistic heavy ion collision, is possible and the topic of current investigations.

An example for an important quantity calculable in thermal perturbative QCD is the gluon self energy. To lowest order it is given by the diagrams shown in Fig.1. Here we are using the following notation:  $P \equiv (p_0, \mathbf{p})$  and  $p \equiv |\mathbf{p}|$ .

At finite temperature these diagrams can be evaluated by using either the imaginary time (Matsubara) or the real time formalism [2,3]. These formalisms amount to a modification of the usual zero temperature Feynman rules in a way to include the thermal distribution functions of the partons. At finite temperature the diagrams of Fig.1, for example, can be evaluated only numerically [4]. However, in the high temperature approximation a closed expression for the one-loop gluon self energy can be found [5,6]. The high temperature limit can be shown to be equivalent to the so-called hard thermal loop (HTL) approximation, introduced by Braaten and Pisarski [7]. Here the diagrams of Fig.1 are computed by assuming the momenta of the internal lines to be much larger than the ones of the external particles. In this way the following result has been obtained:

$$\begin{aligned}\Pi_L(p_0, p) &= -3m_g^2 \left( 1 - \frac{p_0}{2p} \ln \frac{p_0 + p}{p_0 - p} \right), \\ \Pi_T(p_0, p) &= \frac{3}{2}m_g^2 \frac{p_0^2}{p^2} \left[ 1 - \left( 1 - \frac{p^2}{p_0^2} \right) \frac{p_0}{2p} \ln \frac{p_0 + p}{p_0 - p} \right],\end{aligned}\tag{1}$$

where  $\Pi_L \equiv \Pi_{00}$  and  $\Pi_T \equiv \Pi_{ij}(\delta_{ij} - p_i p_j / p^2)/2$  are the longitudinal and transverse components of the gluon self energy and  $m_g^2 = g^2 T^2 (1 + N_f/6)/3$  denotes the effective gluon mass, caused by the interaction with the partons of the plasma. ( $N_f$  is the number of thermalized quark flavors in the QGP.)

It is interesting to note that the expressions given above for the gluon self energy are gauge independent in contrast to the complete one-loop expressions.

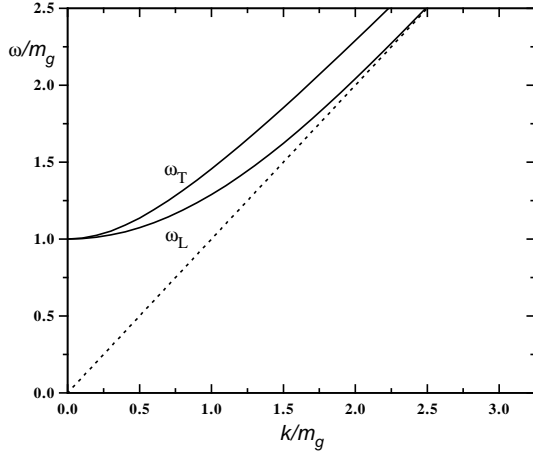


Figure 2. Gluon dispersion relations in a QGP.

An effective gluon propagator can be constructed by resumming the HTL gluon self energy within the Dyson-Schwinger equation, leading to

$$\begin{aligned} D_L^*(P) &= \frac{1}{p^2 - \Pi_L(p_0, p)}, \\ D_T^*(P) &= \frac{1}{P^2 - \Pi_T(p_0, p)} \end{aligned} \quad (2)$$

for the longitudinal and transverse part of the resummed gluon propagator in Coulomb gauge. This propagator describes the propagation of collective plasma modes. The dispersion relation of these plasma modes given by the poles of the propagator is shown in Fig.2. There are two branches, one for the longitudinal plasma mode, also called plasmon, and one for the transverse modes. Both start at the same energy  $m_g$  (plasma frequency) for zero momentum and approach the dispersion relation of a bare gluon at large momenta.

The HTL gluon self energy exhibits an imaginary part for  $p_0^2 < p^2$  leading to Landau damping below the light cone. The HTL plasma modes, however, are not damped as they are situated entirely above the light cone. After all the Landau damping has some interesting consequences as we will discuss below.

In the static limit,  $p_0 = 0$ , the longitudinal HTL gluon self energy reduces to  $m_D^2 = 3m_g^2$ . As a consequence the resummed longitudinal propagator shows Debye screening due to the presence of color charges in the plasma. On the other hand, there is no static magnetic screening in the HTL approximation since  $\Pi_T(p_0 = 0) = 0$ .

## 2. HTL RESUMMATION TECHNIQUE

Restricting to bare propagators perturbative QCD can lead to infrared divergent and gauge dependent results for physical quantities. A famous example is the damping rate  $\gamma$  of a gluon plasma mode at rest, which follows from the imaginary part of the gluon self energy. Using only bare propagators and vertices  $\gamma = a g^2 T / (8\pi)$  has been found with  $a = 1$  in Coulomb or temporal gauge [8] and  $a = -5$  in Feynman gauge [9]. (A negative damping rate corresponds to an unstable QGP.)

The reason for this unphysical behavior can be traced back to the fact that perturbative QCD at finite temperature is incomplete, i.e., higher order diagrams (multi-loop diagrams) can contribute to lower order in the coupling constant [10]. In order to arrive at a consistent expansion at finite temperature, these diagrams, which are exactly the HTL diagrams, have to be resummed into effective propagators and vertices. Besides the effective gluon propagator in (2) there is a resummed quark propagator containing the quark self in the HTL approximation. Furthermore, HTL vertices show up in gauge theories as they are related to the HTL self energies by Ward identities.

Now, assuming that the weak coupling limit,  $\alpha_s \ll 1$ , holds, we see e.g from (1) and (2) that bare propagators are sufficient as long as the momentum is hard,  $p^2 \sim T^2$ . However, for soft momenta,  $p^2 \sim \alpha_s T^2$ , a resummed propagator has to be used. Effective vertices are only necessary if all external legs of the vertex are soft. This is the basic idea of the HTL resummation technique developed by Braaten and Pisarski [7]. In this way consistent results are obtained, i.e., gauge independent results which are complete to leading order in the coupling constant. At the same time the infrared behavior of these quantities is improved due to Debye screening in the resummed gluon propagator.

In the case of the plasmon damping rate at zero momentum the Braaten-Pisarski method leads to the gauge independent result  $\gamma = 6.636 g^2 T / (8\pi)$  [11].

The HTL resummation technique can easily be extended to finite baryon density. For example in the case of the gluon propagator one simply has to replace the effective gluon mass in (1) by [12]

$$m_g^2 = \frac{g^2 T^2}{3} \left[ 1 + \frac{1}{6} \left( N_f + \frac{3}{\pi^2} \sum_f \frac{\mu_f^2}{T^2} \right) \right], \quad (3)$$

where  $\mu_f$  is the chemical potential of the quarks with flavor  $f$ .

Finally, the Braaten-Pisarski method can also be modified to non-equilibrium situations. Basically, one has to replace the thermal distribution functions by non-equilibrium ones (Wigner functions), although some subtleties such as pinch singularities have to be considered [13,14].

### 3. APPLICATIONS

In this section I will discuss the applications of the HTL resummation technique to possible signatures and other interesting observables of a QGP [15].

#### 3.1. Damping rates of energetic partons

The damping rates of quarks and gluons with energies  $E \gg T$  in a QGP are one of the most discussed applications of the Braaten-Pisarski method (for references see [15]).

Within naive perturbation theory, i.e. using only bare Green functions, the damping rate of a hard quark follows from the left diagram of Fig.3, which corresponds to scattering of the energetic quark off the thermal partons via the exchange of a gluon. The matrix element of the scattering diagram is related to the imaginary part of a two-loop quark self energy as can be seen by cutting through the self energy. From these diagrams we expect that the damping rate is of order  $g^4$ . Owing to the exchange of a bare gluon the damping rate in naive perturbation theory turns out to be quadratically infrared divergent.

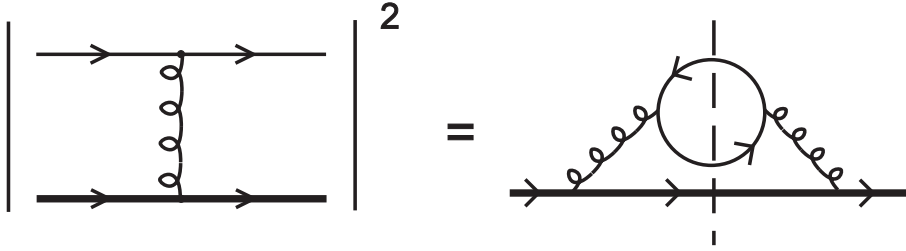


Figure 3. Diagrams for the damping rate within naive perturbation theory.

Using the resummed perturbation theory, the damping to lowest order is derived from the imaginary part of the quark self energy shown in Fig.4 containing a resummed gluon propagator. The imaginary part of this diagram is due to the imaginary part of the HTL gluon self energy of the resummed propagator. Therefore the damping mechanism is caused by the exchange of a virtual plasma mode, which is damped below the light cone (virtual Landau damping).

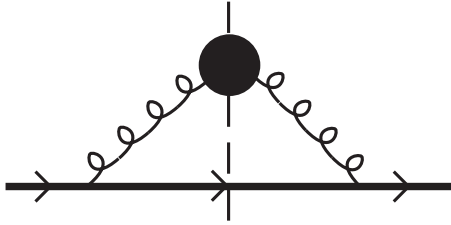


Figure 4. Diagram for the damping rate within resummed perturbation theory.

Computing the damping rate from Fig.4 leads to a logarithmic infrared singularity, which comes from the exchange of the transverse plasma mode containing no static magnetic screening. Hence, in the case of the damping rate of moving partons the HTL resummation method is not sufficient to remove all infrared singularities. Assuming an infrared cutoff of the order  $g^2T$ , which could be provided either by a non-perturbative magnetic mass or by the finite width of the hard quark in the QGP, the following result has been obtained [15]:

$$\gamma_q = \frac{g^2T}{3\pi} \ln \frac{1}{g}. \quad (4)$$

Note that the leading order contribution to the damping rate is of order  $g^2$  in contrast to naive expectation. This anomalous large damping [16] is caused by the use of the resummed gluon propagator, which contains the HTL gluon self energy of order  $g^2$  in the denominator.

A possible physical implication of this damping rate is the color conductivity, which determines the relaxation of the QGP in the case of a small deviation from an equilibrium color distribution. It is given by  $\sigma_c = 4m_g^2/\gamma_g$  [17,18], where  $\gamma_g$  is now the damping rate of a thermal gluon, which follows from (4) by multiplying by a color factor 9/4.

### 3.2. Energy loss of energetic partons

The energy loss of an energetic parton in the QGP is related to jet quenching in ultra-relativistic heavy ion collisions at RHIC and LHC, where jets are expected to arise from high energy partons coming from the primary hard parton collisions. Partons with a large transverse momentum have to propagate through the fireball thereby losing their energy. The amount of jet quenching, produced in this way, may depend on the phase of the fireball and might be used as a signature for the QGP formation therefore [19]. Another application of the energy loss of heavy quarks is the suppression of dileptons with large invariant masses from the decay of charm mesons [20,21].

To lowest order there are two contributions to the energy loss of a parton in the QGP, one coming from elastic scattering (collisional energy loss) and the other one from gluon bremsstrahlung (radiative energy loss). The collisional energy loss can be derived by dividing the energy transfer per collision  $\Delta E$  by the mean free path of the parton. The mean free path due to elastic scattering is proportional to the inverse of the damping rate times the velocity  $v$  of the parton. Therefore the collisional energy loss of a quark, for example, can be calculated from [22]

$$\frac{dE}{dx} = \frac{2}{v} \int d\gamma_q \Delta E. \quad (5)$$

Owing to the additional factor  $\Delta E$  under the integral defining the damping rate the collisional energy loss is only logarithmically infrared divergent within naive perturbation theory and finite using the HTL resummation technique. Using a resummed gluon propagator (Fig.4) for soft momenta of the exchanged gluon and a bare gluon propagator for hard momenta (Fig.3), we end up with an extension of the Bethe-Bloch formula to the case of a QGP [23,24]:

$$\frac{dE}{dx} = \frac{16\pi}{9} \alpha_s^2 T^2 \ln \frac{9E}{16\pi\alpha_s T}. \quad (6)$$

Note that the result is of order  $g^4$  in contrast to the damping rate, which is caused by the reduction of the infrared divergence by the energy transfer factor  $\Delta E$ . Inserting typical values for  $\alpha_s = 0.3 - 0.5$ ,  $T = 200 - 300$  MeV and  $E = 10 - 50$  GeV, we find an energy loss of the order  $dE/dx \simeq 0.5 - 1.5$  GeV/fm. In the case of an energetic gluon we have to multiply this result by 9/4 again. In Fig.5 the collisional energy loss of charm and bottom quarks is shown as a function of the quark momentum for various values of the quark chemical potential [12].

The calculation of the radiative energy loss due to gluon bremsstrahlung is much more involved. For example, the suppression of the gluon emission due to multiple scattering (Landau-Pomeranchuk effect) has to be taken into account. Estimates of the radiative energy loss indicate that it dominates over the collisional one typically by a factor of five [25,26].

### 3.3. Thermalization times and viscosity

In order to estimate thermalization times we have to consider the momentum relaxation in the case of a small deviation from the equilibrium momentum distribution. The momentum relaxation or transport rate is given by

$$\gamma_{trans} = \int d\gamma \frac{\sin^2 \theta}{2}, \quad (7)$$

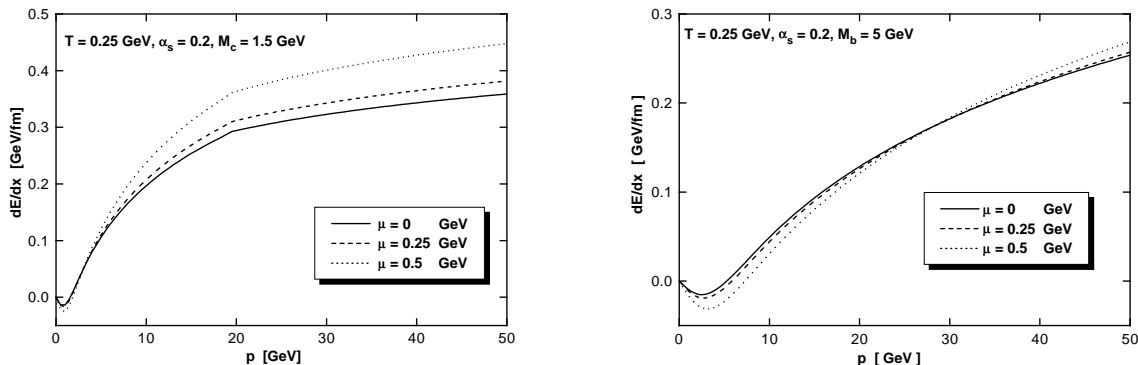


Figure 5. Collisional energy loss of charm and bottom quarks.

where the transport factor  $(\sin^2 \theta)/2$  takes into account that collinear scattering angles  $\theta$  do not contribute to the momentum relaxation.

As in the case of the collisional energy loss the transport factor reduces the degree of the infrared singularity compared to the damping rate, yielding a finite result within the resummed perturbation theory. Calculating the transport rate analogously to the collisional energy loss, the inverse thermalization times,  $\tau^{-1} \equiv 2\gamma_{trans}$ , for quarks and gluons read [27]

$$\begin{aligned}\tau_q^{-1} &= 2.5 \alpha_s^2 T \ln \frac{0.21}{\alpha_s}, \\ \tau_g^{-1} &= 6.6 \alpha_s^2 T \ln \frac{0.19}{\alpha_s}.\end{aligned}\tag{8}$$

This result suggest that gluons thermalize about three times faster than quarks. Hence one might expect that first the gluon component of the primordial parton gas thermalizes and the thermalization of the quark component sets in later [28].

However, the results (8) become unphysical, i.e. negative, for realistic values of the coupling constant,  $\alpha_s > 0.2$ , indicating the break down of perturbation theory. This behavior can be traced back to the use of thermal energies  $E \simeq 3T$  for the partons in (8), whereas for high energies  $E \gg T$ , as in the case of the energy loss (6), reasonable results are found.

The shear viscosity coefficient of the QGP is closely related to the transport rate. Using the relaxation time approximation it is given by  $\eta = (1/15) \epsilon \gamma_{trans}^{-1}$  [29], where  $\epsilon$  is the energy density of the plasma. The viscosity of the QGP is the sum of the viscosities of the gluon and the quark component [27]

$$\eta = \frac{T^3}{\alpha_s^2} \left[ \frac{0.11}{\ln(0.19/\alpha_s)} + \frac{0.37}{\ln(0.21/\alpha_s)} \right].\tag{9}$$

In Fig.6 the viscosity coefficient of the QGP divided by  $T^3$  is shown as a function of the coupling constant. The dashed curve corresponds to an estimate by Baym et al. [30], which is not based on the HTL resummation method. The dotted line indicates the upper limit for the validity of the Navier-Stokes equations [29]. This suggests that dissipation effects are important in the QGP and should not be neglected in hydrodynamical calculations.

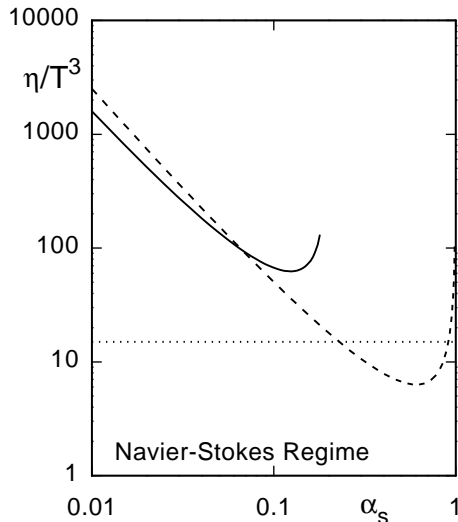


Figure 6. Viscosity coefficient of the QGP.

### 3.4. Photon production

The thermal emission of photons and dileptons from the QGP is one of the proposed signatures for the deconfinement transition [31]. For this purpose one has to know the photon production rate from the QGP as well as from a hadron gas.

Let us first consider hard photons with an energy  $E \gg T$ . To lowest order these photons are produced by the diagrams of Fig.7, i.e. Compton scattering and quark annihilation.

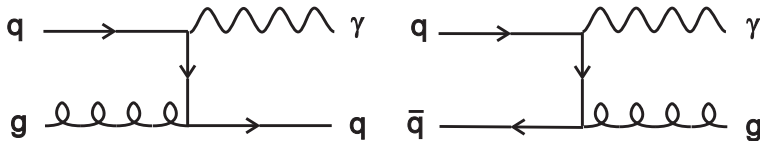


Figure 7. Photon production diagrams in a QGP.

Assuming the quarks to be massless, the diagrams of Fig.7 lead to a logarithmically divergent production rate. Using the resummed quark propagator for soft momenta, on the other hand, a finite result is obtained. (Taking into account the bare quark masses leads also to a finite result, which is, however, much too large because the effective quark masses of the order  $gT$  provide a much larger infrared cutoff.)

The photon production rate from a QGP has been derived using a resummed propagator for soft and a bare one for hard momenta of the exchanged quark [32,33]. In the case of a finite quark chemical  $\mu$  potential the following result has been found [34]:

$$E \frac{dR}{d^3p} = \frac{5\alpha\alpha_s}{18\pi^2} e^{-E/T} \left( T^2 + \frac{\mu^2}{\pi^2} \right) \ln \frac{0.13E}{\alpha_s T}, \quad (10)$$

where  $\alpha$  is the QED fine structure constant.

This rate is of the same order [32] or even two to three times smaller [35,36] than the estimate of the photon production rate from a hadronic gas at the same temperature.



In order to calculate the photon spectrum the space-time evolution of the fireball has to be considered. Using (9) in a hydrodynamical model containing a QGP, a mixed, and a hadronic phase a photon spectrum for SPS ( $S+Au$ ) is found [37] which agrees with the experimental upper limit for the direct photon production [38].

The production rate of soft photons ( $E \ll T$ ) can be calculated from the imaginary part of the one-loop photon self energy containing effective propagators and vertices. Owing to the singularity of the resummed Green functions near the light cone, e.g. for  $p_0 \rightarrow p$  in (1), the soft production rate of on-shell photons exhibits a collinear singularity [39].

### 3.5. Dilepton production

As a last example we consider the production rate of dileptons from the QGP. First we focus on hard dileptons, where the energy  $E$  of the virtual photon is much larger than the temperature. The lowest order contribution of order  $\alpha^2$  comes from the Born term, i.e. the annihilation of a quark-antiquark pair into a virtual photon.

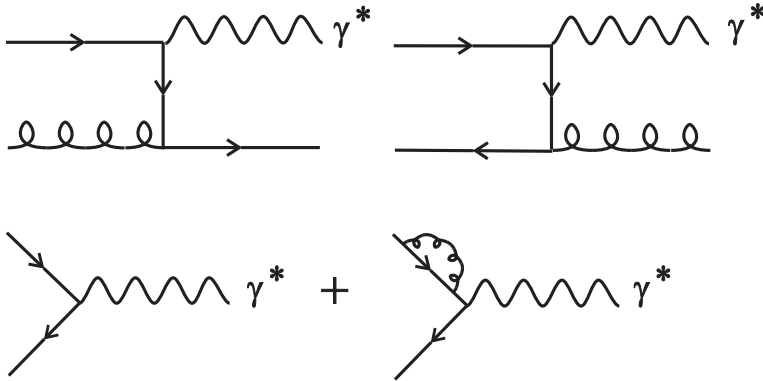


Figure 8.  $\alpha_s$ -corrections of the hard dilepton production in the QGP. The sum of the diagrams in the lower line denote the interference term of these graphs.

For invariant masses  $M^2 \equiv E^2 - p^2 \rightarrow 0$  the Born contribution vanishes. Therefore one has to consider the  $\alpha_s$ -corrections to the dilepton rate for  $M \lesssim T$ . This contribution follows from the diagrams of Fig.8, where besides the graphs leading to the real photon production one has to take into account the interference term of the Born diagram with an annihilation diagram containing a quark self energy insertion. Adding up these contributions the dilepton production rate turns out to be infrared finite even for massless quarks in contrast to the photon rate due to a cancellation of infrared divergences of the interference term and the other diagrams of Fig.8 [40]. However, although the result is finite, one has to use a resummed quark propagator analogously to the real photon case in order to obtain a consistent result. Proceeding similarly to the photon production rate, the following result has been found [41]

$$\frac{dR}{d^4x d^4p} = \frac{10}{27\pi^3} \alpha^2 \alpha_s \frac{T^2}{M^2} e^{-E/T} \left( \ln \frac{T(m_q + k_{min})}{m_q^2} + C \right), \quad (11)$$

where  $m_q^2 = g^2 T^2/6$  is the effective quark mass,  $k_{min} \simeq |Em_q^2/M^2 - M^2/(4E)|$ , and  $C \simeq -0.6$ . This result is shown in Fig.9 as a function of the photon energy  $E$  and

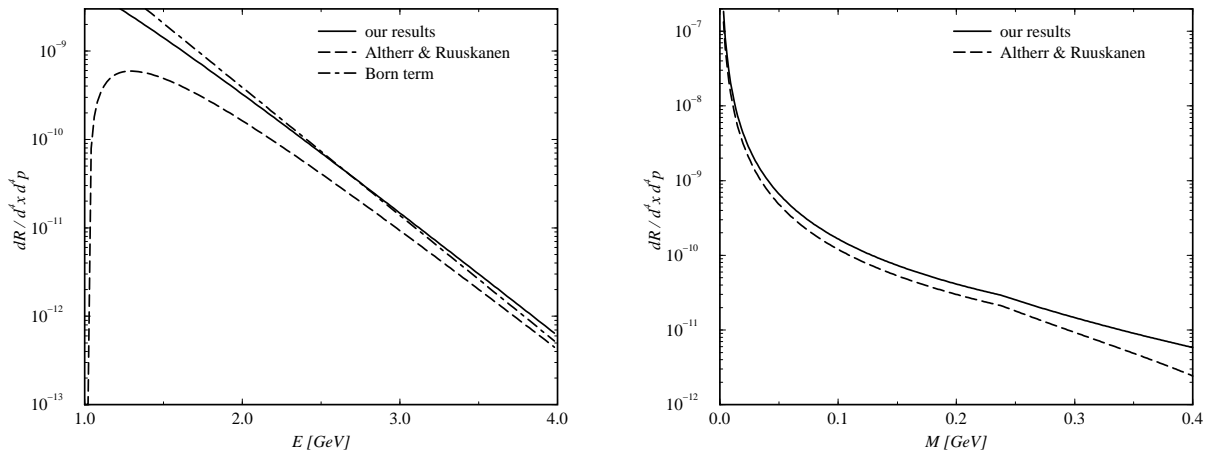


Figure 9. Hard dilepton production rate from the QGP ( $\alpha_s = 0.3$ ,  $T = 300$  MeV) as a function of  $E$  for  $M = 300$  MeV (left figure) and as a function of  $M$  for  $E = 3$  GeV (right figure).

the invariant mass  $M$  for  $\alpha_s = 0.3$ ,  $T = 300$  MeV. For comparison the result found by Altherr and Ruuskanen [40] calculated with bare propagators and the Born contribution are shown. For smaller invariant masses the  $\alpha_s$ -corrections dominate over the Born term, which is independent of  $M$ . For example, for  $M = 100$  MeV and  $E = 3$  GeV the  $\alpha_s$ -correction exceeds the Born contribution by a factor of about 20.

The production rate of soft dileptons can be derived from the same photon self energy as the soft photon production [42,43]. However, due to the off-shellness of the photons there is no collinear infrared singularity in this case. The soft photon production shows an interesting structure as a function of the photon energy caused by the dispersion relation of the soft quark modes in the QGP [42].

#### 4. CONCLUSIONS

Using perturbative QCD at finite temperature static as well as dynamical properties of a QGP can be calculated. This method can be extended in a straightforward manner to finite baryon density, i.e. finite quark chemical potential, and even to non-equilibrium situations using the Keldysh formalism. Perturbative QCD is expected to work at high temperatures, where the effective strong coupling constant becomes small due to asymptotic freedom. However, using only bare propagators and vertices infrared divergent and gauge dependent results are obtained even for physical quantities. Using, however, HTL resummed Green functions for soft momenta of the order  $gT$  and smaller, consistent results can be derived, i.e. gauge independent results complete to leading order in the coupling constant. In many cases all infrared singularities are removed to leading order in the coupling constant in this way. At the same time important medium effects of the QGP, such as effective parton masses, Debye screening, and Landau damping, are taken into account.

The HTL resummation technique has been applied to the following observables of the

QGP:

1. Damping rates of quarks and gluons in the QGP, which are related to color conductivity of the QGP.
2. The energy loss of energetic partons in the QGP, which determines the amount of jet quenching at RHIC and LHC and the suppression of high invariant mass dileptons from the decay of charm mesons.
3. Thermalization times of quarks and gluons, which show that gluons equilibrate faster than quarks.
4. The viscosity of the QGP indicating the significance of dissipative effects in the QGP.
5. Photon and dilepton production rates, which serve as a promising signature for the QGP formation.

There are two open problems concerning the application of the HTL resummation technique. The first one is the weak coupling limit ( $\alpha_s \ll 1$ ), which had been assumed in the derivation of the HTL method. For realistic values of the coupling constant the HTL calculations to lowest order fail if the energy of the quantity under consideration is of the order of the temperature or smaller. Examples are the Debye mass, which is about a factor of three smaller than the one obtained non-perturbatively [44,45], and the thermalization times and the viscosity discussed here, which become negative for  $\alpha_s > 0.2$ . For large energies ( $E \gg T$ ), on the other hand, the HTL resummation technique produces reasonable results, such as the collisional energy loss of energetic partons and the production rates of hard photons and dileptons.

The second problem concerns infrared singularities. Although the inclusion of Debye screening using the HTL method reduces the infrared singularities to a large extent compared to naive perturbation theory, two classes of singularities still survive. The first one is caused by the absence of static magnetic screening in the HTL resummed gluon propagator. Either a magnetic screening mass or a finite width of the partons in the QGP can cure this problems. Magnetic screening masses require the use of non-perturbative methods [46], while a finite width of the thermal partons can be achieved by a Bloch-Nordsieck resummation [47]. The second cause for possible infrared singularities is the divergence of the resummed Green functions at the light cone. In the case of the soft photon production this leads to a collinear infrared singularity. In order to remove this singularity an improved HTL resummation scheme has been proposed [48].

## REFERENCES

1. A. Ukawa, these proceedings.
2. J.I. Kapusta, Finite-Temperature Field Theory, Cambridge University Press, Cambridge, 1989.
3. M. Le Bellac, Thermal Field Theory, Cambridge University Press, Cambridge, 1996.
4. A. Peshier, K. Schertler, and M.H. Thoma, hep-ph/9708434, to be published in Ann. Phys. (N.Y.).
5. V.V. Klimov, Sov. Phys. JETP 55 (1982) 199.
6. H.A. Weldon, Phys. Rev. D 26 (1982) 1394.
7. E. Braaten and R.D. Pisarski, Nucl. Phys. B 337 (1990) 569.
8. K. Kajantie and J.I. Kapusta, Ann. Phys. (N.Y.) 160 (1985) 477.

9. J.A. Lopez, J.C. Parikh, and P.J. Siemens, Texas A&M preprint, 1985 (unpublished).
10. R.D. Pisarski, Phys. Rev. Lett. 63 (1989) 1129.
11. E. Braaten and R.D. Pisarski, Phys. Rev. D 42 (1990) 2156.
12. H. Vija and M.H. Thoma, Phys. Lett. B 342 (1995) 212.
13. R. Baier et al., Phys. Rev. D 56 (1997) 2548.
14. M.E. Carrington, H. Defu, and M.H. Thoma, hep-ph/9708363.
15. M.H. Thoma, in: Quark-Gluon Plasma 2, ed. R.C. Hwa, World Scientific, Singapore, 1995, p.51.
16. V.V. Lebedev and A.V. Smilga, Ann. Phys. (N.Y.) 202 (1990) 229.
17. A.V. Selikhov and M. Gyulassy, Phys. Lett. B 316 (1993) 373.
18. H. Heiselberg, Phys. Rev. Lett. 72 (1994) 3013.
19. M. Gyulassy and M. Plümer, Phys. Lett. B 243 (1990) 432.
20. Z. Lin, R. Vogt, and X.N. Wang, nucl-th/9705006.
21. M.G. Mustafa et al., nucl-th/9711059.
22. E. Braaten and M.H. Thoma, Phys. Rev. D 44 (1991) 1298.
23. E. Braaten and M.H. Thoma, Phys. Rev. D 44 (1991) 2625.
24. M.H. Thoma, Phys. Lett. B 273 (1991) 128.
25. M. Gyulassy and X.N. Wang, Nucl. Phys. B 420 (1994) 583.
26. R. Baier et al., Phys. Lett. B 345 (1995) 277.
27. M.H. Thoma, Phys. Rev. D 49 (1994) 451.
28. E. Shuryak, Phys. Rev. Lett. 68 (1992) 3270.
29. P. Danielewicz and M. Gyulassy, Phys. Rev. D 31 (1985) 53.
30. G. Baym et al., Phys. Rev. Lett. 64 (1990) 1867.
31. P.V. Ruuskanen, Nucl. Phys. A 544 (1992) 169c.
32. J.I. Kapusta, P. Lichard, and D. Seibert, Phys. Rev. D 44 (1991) 2774.
33. R. Baier et al., Z. Phys. C 53 (1992) 433.
34. C.T. Traxler, H. Vija, and M.H. Thoma, Phys. Lett. B 346 (1995) 329.
35. L. Xiong, E. Shuryak, and G.E. Brown, Phys. Rev. D 46 (1992) 3798.
36. K. Haglin, Phys. Rev. C 50 (1994) 1688.
37. N. Arbex et al., Phys. Lett. B 345 (1995) 307.
38. A. Drees, Nucl. Phys. A 610 (1996) 536c.
39. R. Baier, S. Peigné, and D. Schiff, Z. Phys. C 51 (1991) 581.
40. T. Altherr and P.V. Ruuskanen, Nucl. Phys. B 380 (1992) 377.
41. M.H. Thoma and C.T. Traxler, Phys. Rev. D 56 (1997) 198.
42. E. Braaten, R.D. Pisarski, and T.C. Yuan, Phys. Rev. Lett. 64 (1990) 2242.
43. S.M.H. Wong, Z. Phys. C 53 (1992) 465.
44. U.M. Heller, F. Karsch, J. Rank, hep-lat/9710033.
45. K. Kajantie et al., Phys. Rev. Lett. 79 (1997) 3130.
46. A. Lindé, Phys. Lett. 96 B (1980) 289.
47. J.P. Blaizot and E. Iancu, Phys. Rev. D 56 (1997) 7877.
48. F. Flechsig and A.K. Rebhan, Nucl. Phys. B 464 (1996) 279.